Polymer 295 (2024) 126771

Contents lists available at ScienceDirect

Polymer

journal homepage: www.elsevier.com/locate/polymer

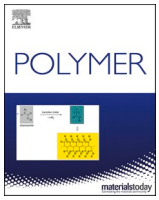

Microstructural investigation of the cooperative gelation of syndiotactic polystyrene and high M_W polyethylene glycol di-methyl ether in common solution in THF

Fumitoshi Kaneko [a], Maria-Maddalena Schiavone [b], Hiroki Iwase [c], Shin-ichi Takata [d], Jürgen Allgaier [e], Aurel Radulescu [b,*]

[a] Graduate School of Science, Osaka University, 1-1 Machikaneyama, Toyonaka, Osaka, 560-0043, Japan
[b] Jülich Centre for Neutron Science (JCNS), Heinz Maier-Leibnitz Zentrum (MLZ), Lichtenbergstrasse 1, 85748, Garching, Germany
[c] Neutron Science and Technology Centre, Comprehensive Research Organization for Science and Society CROSS, Tokai, 319-1106, Japan
[d] Materials and Life Science Division, Japan Proton Accelerator Complex J-PARC, Tokai, 319-1195, Japan
[e] Jülich Centre for Neutron Science (JCNS), Forschungszentrum Jülich GmbH, Jülich, 52425, Germany

A B S T R A C T

The gelation of syndiotactic polystyrene (sPS) in THF in the presence of high molecular weight PEGDME was investigated in detail using contrast-matching SANS complemented by in situ FTIR. Using the contrast-matching method, the scattering contribution of each of the two polymers in the common solution in THF at high temperature (110 °C), in the single-coil conformational state and in the gelation state of sPS (below 40 °C and down to 10 °C) was observed, and the structural characterization of the polymer coils and the junction structures of the gel was obtained. The local scale conformation of the two types of polymer molecules in the different regimes was additionally monitored by FTIR. The gelation and melting temperatures were determined by DSC. sPS changes from the amorphous coil to the helical TTGG conformation when the gelation temperature is passed, forming fibrillar morphologies with a local 2D aspect due to cooperative interactions with the solvent molecules. These are the junction structures of the large-scale network morphology of the gel. The high molecular weight PEGDME transitions from the amorphous coil to an elongated amorphous conformation and incorporates into the fibrillar morphology together with the sPS during the gelation process. High M_W PEGDME alone in THF forms a "house of cards" gel consisting of stacked lamellar structures on a smaller length scale, as shown by the scattering data. Thus, in the presence of sPS, smaller and softer structures appear as a result of a cooperative gelation process controlled by sPS. Incorporation of high M_W PEGDME into these aggregates leads to polymer nanocomposites that can render the sPS hydrophilic, a topic that should be the focus of future structural and morphological studies.

1. Introduction

Syndiotactic-polystyrene (sPS) is a relatively new material [1] that shows a complex polymorphic behavior, including five different crystalline forms in which the chains adopt either a planar zig-zag (α- and β-form) or a TTGG helical (γ-, δ- and ε-form) conformation [2–4]. sPS is also able to form different kinds of co-crystalline (clathrate) phases with a large number of small organic molecules which can be incorporated as guests in the cage- or channels-like cavities between the polymer helices of the δ- and ε-forms, respectively [5–7]. Solvent-induced crystallization by using either the film casting from solution or the exposure of amorphous films to solvents in vapor or liquid state leads to formation of helical co-crystalline δ and ε forms, depending on the solvent type. Moreover, the initial guest molecules in sPS co-crystals can be replaced smoothly with other kind of molecules by exposure to vapors or liquid [8,9]. The guest exchange procedure has the advantage to enable sPS to form co-crystals even with chemical compounds that are difficult to incorporate into the crystalline region by usual solution-cast and solvent-induced crystallization methods. Following suitable guest extraction procedures emptied clathrate forms of s-PS (δ_e- or ε_e-forms) may also be obtained, which correspond to pure helical form of s-PS free from the guest molecules. The δ_e empty form is different from the γ-form, which is also a pure helical form that is free of guest molecules, and is obtained either by annealing or heating the clathrate δ form in the temperature range 110–170 °C, which purges away the solvent molecules and yields closely packed helical chains in the crystal lattice [10]. The clathrate forms are interesting for applications, when active guests can be incorporated in the sPS films, leading to advanced materials for optical and magnetic applications [11–14], while the emptied clathrates can find application as molecular sieves [15], for water purification from chlorinated hydrocarbons.

It has been found that chemical compounds consisting of ethylene

* Corresponding author.
E-mail address: a.radulescu@fz-juelich.de (A. Radulescu).

https://doi.org/10.1016/j.polymer.2024.126771
Received 20 November 2023; Received in revised form 31 January 2024; Accepted 5 February 2024
Available online 7 February 2024

oxide repeat units $(C_2H_4O)_n$ seem to possess sufficient affinity to become a guest of sPS co-crystals via guest exchange procedure. This was confirmed in linear polyethylene glycols (PEGs) with molecular weight (M_W) up to 1000 g/mol [16]. To answer the question of how such long-chain compounds can be introduced into the crystalline cavities of the sPS lattice and what conformation they adopt, it is desirable to obtain information on the general molecular shape and local molecular structure of PEGs. This was elucidated in the case of the co-crystal systems of sPS and short polyethylene glycol dimethyl ether (PEGDME) or triethylene-glycol dimethyl ether (TEGDME) by a simultaneous experimental approach combining measurements by small-angle neutron scattering (SANS) and Fourier-transform infrared (FTIR) spectroscopy [17], with the film samples prepared by applying the guest exchange procedure between the initial guest ($CHCl_3$) and the final guest (PEGDME or TEGDME). However, although the guest exchange procedure is a useful method applicable for a variety of chemical compounds, there is a practical problem for the co-crystallization of sPS with PEG: the higher the molecular weight of the PEG guest, the longer the time required for this procedure, which is attributable to a significant decrease in the diffusivity of PEG with increasing molecular weight. Accordingly, it is unrealistic to adopt the guest exchange procedure for the preparation of sPS co-crystals containing high-molecular weight PEG. Recently it was found that sPS cocrystal films containing n-alkyl carboxylic acid (n-CA) could be manufactured not only by applying the guest exchange procedure to sPS cocrystal films but also by casting a chloroform ($CHCl_3$) solution containing two solutes, namely, the host sPS and the guest n-CA [18]. Taking into account that solvent molecules are often embraced in the crystalline region as guests when sPS films are prepared by casting from solution, it is reasonable that a chemical species dissolved as a co-solute is taken into the crystalline region if its affinity to the cavity of the sPS cocrystal lattice is larger than that of the solvent molecule, as in the case of chemical compounds consisting of ethylene oxide repeat units. Therefore, a new manufacturing process for sPS/PEG cocrystal film formation was tested recently by casting binary solute solutions of the two components at different weight ratios in $CHCl_3$ [19]. It was concluded that the procedure may be applicable PEG with molecular weight as high as 20000 g/mol. According to previous studies [20] the PEG molecules are distributed not only in the crystalline region but also in the amorphous region, therefore in the case of high Mw PEG involved in the sample preparation it may be considered that parts of the PEG chain may be included in the amorphous region.

On the other hand, the thermoreversible gelation of highly stereoregular polymers such as sPS proceeds in two steps [21,22]: a first step is an intramolecular coil-to-TTGG helix transition by clustering of several chain segments or by organization of a single chains segment, which is followed by an intermolecular association of multiple helix segments that leads to the formation of the network structure. The gel properties depend on the structure of the junction zones of starting gel. Depending on solvent type and/or thermal history, two kinds of gels were reported, elastic gels that are characterized by helical chain conformation and paste-like opaque gels characterized by *trans*-planar zigzag chain conformation. Moreover, it was shown [23–26] that the characteristic shared by these thermoreversible gels is the existence of fibre-like structures that seem to imply the absence of chain folding. sPS would then produce fibrillar physical gels owing to helix stabilization by the solvent molecules that suppresses chain folding and promotes formation of crystalline phase with preferentially fibrillar morphology. It was also demonstrated by XRD [27,28] and neutron diffraction (ND) and SANS [24,25] experiments that the structure of sPS fibrils in the gel form is identical to that in the sPS δ co-crystalline phase (clathrates and intercalates).

Studies of gelation of s-PS in dichloroethane (DCE) in the presence of low M_W PEG indicated that an increase of the PEG content in the gel led to change the structure of s-PS from a helical conformation to a *trans*-zigzag one [29]. Another work has shown that when PEG is dissolved along with the sPS in THF and sPS is allowed to undergo thermoreversible gelation a PEG-rich solution formed separate domains inside the gel, of a size that is a function of the concentration and M_W of PEG [30]. However, the interaction mechanism between the sPS and high M_W PEG molecules in the transition from solution to gel state is still a subject that requires further investigations.

In this work, we report the characterization of the physical gelation of sPS in the presence of high molecular weight PEGDME from THF solution by contrast variation SANS. The choice for PEGDME was to avoid clustering effects, which, as reported in Ref. [31], depend of the polymer chain end groups. Formation and evolution of the structure and morphology at different gelation temperatures in transition from the single-coil conformation of the two polymer species at 110 °C to the ordered regular conformational of sPS in gel phase is additionally characterized by FTIR analysis of the samples simultaneously with SANS. The cooperative gelation process of sPS and high molecular weight PEGDME in common solution in THF is discussed in a parallel analysis of the structure and morphology formed by the two polymer species when present alone in THF solution. The formation and melting temperatures of sPS and PEGDME gels in common and individual solution in THF were determined by DSC, which provided the reference for the temperature around which the detailed analysis of the conformational change between the single coil and the regular form of sPS as a function of solution composition was conducted.

2. Experimental

2.1. Materials and sample preparation

Syndiotactic polystyrene (sPS) (weight average molecular weight $M_W = 1.1 \times 10^5$ g/mol and dispersity 1.9) was synthesized in both protonated (h-sPS) and deuterated (d-sPS) states according to the coordination polymerization developed by Ref. [1], using styrene monomers with a purity higher than 98% purchased from Cambridge Isotope Laboratories. PEGDME with $M_W = 2$ x 10^4 and 4×10^4 g/mol were synthesized in house in both protonated (h-PEGDME) and deuterated (d-PEGDME) states using anionic polymerization and characterized by size exclusion chromatography [32]. Tetrahydrofuran (THF) was purchase in both protonated (h-THF) and deuterated (d-THF) states from Sigma–Aldrich and used without further purification.

For the study of gelation of sPS and PEGDME from common solution in THF and structure and morphology analysis, the polymers were mixed in proper amounts in THF to obtain final solutions with 5% sPS and 1% PEGDME v/v%, respectively. PEGDME of 20K and 40K were considered for the structural study. For the gelation and melting analysis with DSC the solutions were prepared for 5% sPS and 3% PEGDME v/v% in THF. sPS and PEGDME40K were also investigated separately in THF solution. The small angle scattering of neutrons arises from the fluctuations of the scattering length density (SLD) within the sample. For a ternary system containing THF, sPS and PEGDME, the macroscopic cross-section can be expressed in terms of the partial structure factors as

$$\begin{aligned} d\Sigma/d\Omega(Q) = {} & (\rho_{sPS} - \rho_{THF})^2 \, S_{sPS\text{-}sPS}(Q) \\ & + 2\,(\rho_{sPS} - \rho_{THF})(\rho_{PEGDME} - \rho_{THF})\, S_{sPS\text{-}PEGDME}(Q) \\ & + (\rho_{PEGDME} - \rho_{THF})^2 \, S_{PEGDME\text{-}PEGDME}(Q) \end{aligned} \quad (1)$$

The partial scattering functions contain structural information about the sPS and PEGDME in their solute or aggregated state and their mutual interaction. This information in principle may be accessed separately by proper variation of the SLDs of the components in the ternary system (Table 1) by D-labelling, thereby varying the contrast factors in Eq. (1). In order to achieve the neutron contrast matching conditions between one polymer species and the solvent in the initial solution and to keep the incoherent level at lowest level the following combination schemes were used to specifically enable only one polymer species "visible" while rendering the other one "invisible" in the SANS experiments: (i) h-sPS and d-PEGDME in d-THF that enabled the sPS visible; (ii) d-sPS and h-

Table 1
Summary of all samples and their neutron scattering length density.

Sample	SLD [10^{-6} Å^{-2}]
h-PEGDME	0.64
d-PEGDME	6.90
h-sPS	1.40
d-sPS	6.42
h-THF	0.20
d-THF	6.35

PEGDME in d-THF for the PEGDME visible; (iii) h-sPS and h-PEGDME in d-THF to have both polymers visible.

The polymer solutions were prepared in tightly sealed sample cells made of bras and equipped with ZnSe windows, allowing a beam path of 1 mm.

2.2. Measurements

For simultaneous SANS/FTIR measurements, an experimental setup combining a compact portable FTIR spectrometer (PerkinElmer, Spectrum Two) and an optical system that plays the role of beam mixer and selector was used. The optical system consists of a set of mirrors that allows the extraction of the IR beam out of the spectrometer, enabling the coaxial irradiation of sample by both the neutron and the IR beams, and the reflection of the scattered IR beam back to the spectrometer, while enabling the scattered neutrons to arrive onto the neutron detector placed at different distances from the sample. A detailed description of the experimental setup can be found elsewhere [17].

During simultaneous SANS and FTIR experimental investigation the samples were heated in-situ at about 110 °C (well above the boiling points of THF) and then cooled down to different temperatures using an oil bath controlled from the SANS measurement software. SANS and FTIR characterizations were carried out simultaneously at different gelation temperatures, where a translucent gel was yielded. Empty sample container and solvent sample was prepared and measured additionally.

The simultaneous SANS/FTIR measurements were carried at the BL15 beamline (the small and wide-angle neutron diffractometer TAIKAN) at J-PARC, Tokai, Japan [33] and at the KWS2 diffractometer of the Jülich Centre for Neutron Science (JCNS) at Heinz Maier-Leibnitz Zentrum (MLZ), Garching, Germany [34]. At TAIKAN using the time-of-flight method with a wide wavelength band (λ from 0.7 to 8 Å) a Q-range between 0.005 and 5 Å^{-1} may be covered using the small-, middle- and wide-angle detectors. At KWS-2 the pinhole SANS method with λ = 5 Å and neutron acquisition with the main detector placed at different detection distances between 2 m and 20 m after the sample enables a Q-range between 0.001 and 0.6 Å^{-1}. Additional SANS measurements were carried out on selected samples and conditions at KWS-2 using the pinhole mode with a longer wavelength λ = 20 Å and the focusing mode with neutron lenses and a secondary high-resolution detector [35], which enabled to reach the Q_{min} = 2 x 10^{-4} Å^{-1}.

The measured two-dimensional SANS data were subjected to typical corrections for the empty cell contribution, instrumental background and detector sensitivity, calibrated in absolute units of cm^{-1} by using the secondary standard sample of glassy carbon at TAIKAN and of Plexiglas at KWS-2, and radially averaged to deliver the one-dimensional scattering intensity I(Q).

Transmission IR spectra were taken simultaneously with SANS with a resolution of 2 cm^{-1} at 1 min intervals. For measuring the time dependence of IR spectra and analyzing them, commercially available software (PerkinElmer, Timebase) was employed.

DSC characterizations of a h-sPS solution in h-THF and a common h-sPS and h-PEGDME solution in h-THF were carried out using a differential scanning microcalorimeter Setaram DSC131 EVO and samples sealed in stainless steel crucibles. The gels obtained by pre-cooling homogeneous solutions in THF from 110 °C for sPS and mixed sPS-PEGDME and from 50 °C for PEGDME were transferred to sample crucibles. Samples were heated to the highest target temperature (110 °C if sPS was present, 50 °C otherwise) and DSC scans were performed under a nitrogen atmosphere at a cooling/heating rate of 5 °C/min while samples were cooled to the gel phase, followed by heating to observe the melting of the gel.

3. Results

The DSC thermograms with cycled cooling/heating procedure of the sPS and of PEGDME40K individual solutions in THF and of sPS and PEGDME40K common solution in THF for the polymers volume fraction in solution of φ_P = 5% and 3% for sPS and PEGDME40K, respectively, are shown in Fig. 1. Formation of sPS gel in THF occurs at around T_c = 35 °C, while its melting takes place at higher temperatures over a broader range between 70 °C and 80 °C. Gelation of h-PEGDME40K in THF appears at 25 °C, while the melting at around 20 °C. The common solution of sPS and PEGDME40k in THF shows only one gelation peak, at around T_c = 40 °C, while in melting two process can be observed: the first one takes place at around 20 °C and can be assigned to melting of PEGDME40K gel, while the second that appears over a broader range of higher temperatures, between 75 °C and 85 °C, corresponds to the melting of sPS gel. The behavior of the sample containing both polymers in common THF solution with only one gelation peak and two melting peaks is characteristic of the co-assembly of the two polymer species, with the melting occurring at the characteristic temperature T_m of each species, as observed for other systems too [36,37].

Fig. 2a shows the experimental SANS patterns measured on h-PEGDME20K solutions in d-THF for different polymer volume fractions φ_P at 30 °C. For the most dilute sample (φ_P = 0.25%) the power law exponents (Q^{-p}) specific for different morphologies of the polymer at different length scales in solution are indicated. At small Q, where the Guinier region is observed, the radius of gyration R_g of the polymer coil can be determined. At medium Q, a characteristic decay exponent indicates the quality of the solvent: chains in a theta solvent without interaction with excluded volume form Gaussian coils with a characteristic decay p = 2 of the scattering intensity, while chains with excluded volume in a good solvent, such as PEO in THF [38], give an exponent p = 5/3. For semiflexible polymer chains, a transition to Q^{-1} behavior follows at higher Q, whereby the polymer chain looks like a

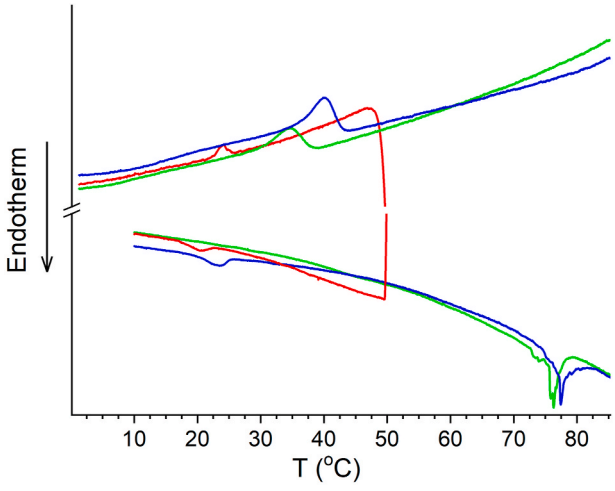

Fig. 1. Thermal behavior of the samples consisting of 5 % h-sPS and 3 % h-PEGDME40K in common h-THF solution (blue line), 5 % h-sPS in h-THF solution (green line) and 3 % h-PEGDME40K in h-THF solution (red line), determined by DSC during the melting and gelation processes. (For interpretation of the references to colour in this figure legend, the reader is referred to the Web version of this article.)

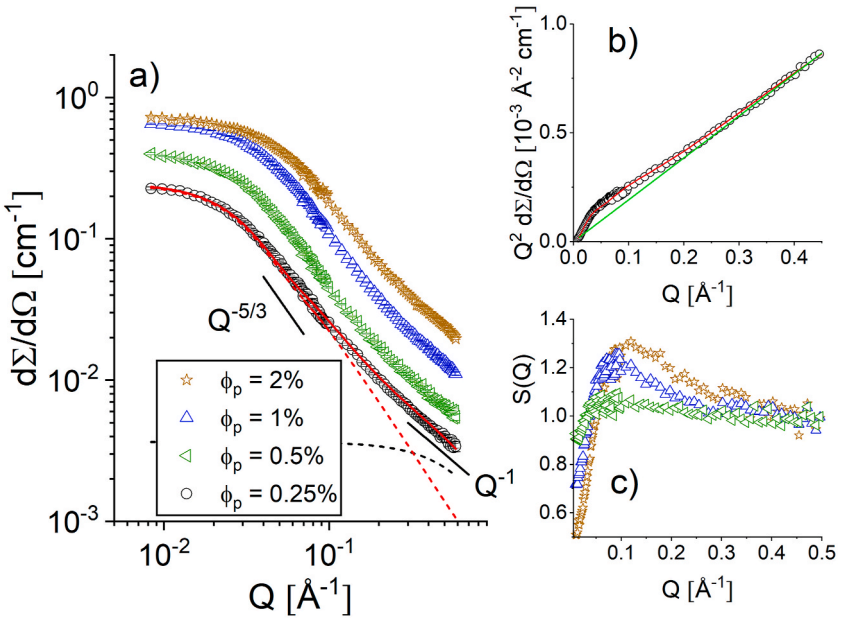

Fig. 2. Small angle scattering cross sections measured at 30 °C from a solution of h-PEGDME20k in d-THF at different polymer volume fractions φ_p in solution, in a log-log presentation (a), the Kratky-plot presentation of the scattering results obtained for $\varphi_p = 0.25$ % (b) and the structure factor that characterizes the scattering of highly concentrated samples (c). The solid black lines in panel (a) show the power-law behavior of the scattering intensity in different Q-ranges, the solid red line depicts the model interpretation of the data for the lowest polymer concentration, as described in the text, while the dotted lines represent the contributions of the two structural levels considered in the model. The solid red line in panel (b) has the same meaning as in panel (a), while the green line indicates the signal from a rod-like morphology (see text). (For interpretation of the references to colour in this figure legend, the reader is referred to the Web version of this article.)

rod-like segment on the length scale of the persistence length l_P. A polymer chain that gives rise to such scattering features in SANS or SAXS can be described by the persistent wormlike chain model established by Kratky and Porod [39]. Such polymer chains are characterized by long- and short-range interactions and consist of average linear segments of a certain length, $l_K = 2\ l_P$, where l_K is the Kuhn step length, and a certain cross-sectional area A_K, i.e. the two-dimensionally averaged, cross-sectional radius of gyration R_C orthogonal to the contour length of the chain. l_K refers to the contour length L of the polymer chain by $L = n_K\ l_K$, where n_K is the number of Kuhn units in the chain. A high molecular weight PEGDME chain in dilute solution can therefore be treated with the Kratky-Porod model of a wormlike chain for a persistent chain. Alternatively, it can be generally assumed that in a freely jointed chain, rod-like segments of length l_K form a polymer chain of fractal mass dimension $d_f = 5/3$ or $d_f = 2$ for the polymer in good or theta solvent, respectively, as proposed by Beaucage [40]. The interpretation of the scattering pattern for $\varphi_P = 0.25\%$ using the proposed unified function [41,42] was done by considering the contribution of two structural levels, namely the overall dimension (radius of gyration) of the coil and the substructural level l_P, as used in other similar structural studies [43]. The unified equation applied to the two structural levels of a persistent Kratky-Porod chain is given by:

$$I(Q) = \left\{ G_2\ exp\left(-\frac{Q^2 {R_{g2}}^2}{3} \right) + B_2\ exp\left(-\frac{Q^2 {l_p}^2}{3} \right) \left(q_2^*\right)^{-d_{f2}} \right\} +$$

$$\left\{ G_1\ exp\left(-\frac{Q^2 {R_{g1}}^2}{3} \right) + B_1\ exp\left(-\frac{Q^2 {R_c}^2}{3} \right) \left(q_1^*\right)^{-d_{f1}} \right\} \quad (2)$$

where

$$q_n^* = \left[\frac{Q}{\left\{ erf\left(1.06 Q R_g/\sqrt{6}\right) \right\}^3} \right] \quad (3)$$

for the two structural levels under consideration n = 1, 2.

The first bracket and the subscript "2″ in Eq. (2) refer to the Guinier regime in the low Q range, starting from the observed plateau and the bending of the scattering profile to high Q. The second bracket and the subscript "1″ describe the persistent rod-like scaling regime. The fractal mass dimensions of the considered structural levels are described by the exponent d_f, namely $d_f = 5/3$ or $d_f = 2$ for the polymer in good or theta solvent or $d_f = 1$ for the rod-like morphology. A third term (the component "0″) can be added to Eq. (2) if the scattering due to a different local structural level is observed at very high Q values resulting from the cross-sectional radius of persistence

$$\left\{ G_0\ exp\left(-\frac{Q^2 {R_c}^2}{3} \right) + B_0 \left(q_0^*\right)^{-4} \right\} \quad (4)$$

G_2 is the Guinier pre-factor ("forward-scattering") and R_{g2} is the radius of gyration characterising the Guinier regime. For the persistent rodlike scaling regime $G_1 = G_2/n_K$ and R_{g1} is defined as

$$R_{g1} = \sqrt{\frac{{l_P}^2}{3} + \frac{{R_c}^2}{2}} \quad (5)$$

The pre-factor G_0 is defined as $G_0 = G_1\ (R_c/(2l_P))^2$, as described in Refs. [41,42]. Finally, the pre-factors B_0 is the Porod pre-factor for a rod structure of length $2l_P$, while B_1 and B_2 relate to G_1 and R_{g1} and G_2 and R_{g2}, respectively, as described in Ref. [43] in details.

However, due to the limited Q range in our experiment, the length scale characteristic of the n = 0 structure level could not be reached. Therefore, the experimental data were characterized by the model described in Eq. (2). The red curve in Fig. 2 shows the result of the model fit. The contribution of the two structural levels considered is indicated by the dashed red and black lines. The model interpretation of the experimental data yielded the most important quantities for the structural characterisation of the high M_W PEGDME in THF, namely the sizes $R_{g2} = 52.7$ Å and $l_P = 4.75$ Å as well as the forward scattering of the polymer in solution $I_0 = G_2 = 0.245$ cm^{-1}. The "forward scattering" of an ensemble of protonated polymer coils dissolved with a volume fraction φ_P in deuterated solvent is defined as $I_0 = \varphi_P\ \Delta\rho^2\ V_m$, where $\Delta\rho$ is the neutron contrast representing the difference in SLD between the

protonated polymer and the deuterated solvent, and V_m is the molar volume of the polymer chain. The calculation of the "forward scattering" from a volume fraction φ_P = 0.25% of h-PEGDME20K in d-THF considering the SLDs from Table 1 and a polymer mass density of 1.125 g cm^{-3} resulted in a value of the "forward scattering" of I_0^{calc} = 0.240 cm^{-1}, which is very close to the measured and fitted values. Fig. 2b shows in a Kratky plot the scattering data of the lowest polymer concentration in THF and the fit results according to Eq. (2) represented by the red curve. The peculiarities of a Kratky-Porod chain can be clearly seen when compared with the feature of a rod-like morphology, as indicated by the green line resulting from fitting the high Q portion of the experimental results with a Q^{-1} power law.

As the volume fraction of the polymer in solution increases, correlation effects between the polymer coils contribute to the scattering intensity, as shown in Fig. 2c, as evidenced by the structure factor S(Q). Typically, the scattering intensity of an ensemble of concentrated scattering centers, such as polymer coils in solution, is expressed as $I(Q) = I_0$ P(Q) S(Q), where P(Q) represents the form factor of the polymer coil, which reflects the intraparticle correlations, while S(Q) represents the structure factor arising from the interparticle correlations. At low φ_P, in the dilute regime, S(Q) = 1, while with increasing φ_P S(Q) starts to become significant. S(Q) can be determined by dividing I(Q) measured for a high φ_P by the intensity of the highly diluted particle ensemble, which is shown in Fig. 2, considering that S(Q) = 1 for φ_P = 0.25 %. For the highest volume fraction φ_P = 2 %, a correlation distance of about 60 Å between the polymer coils can be estimated from the evaluation of the peak position in S(Q).

The SANS scattering patterns of sPS and PEGDME20k individual solutions in d-THF at two temperatures, 110 °C and 35 °C, above and just before the gelation point of the sPS in solution are shown in Fig. 3 in parallel with the SANS patterns of the two polymers in common solution in d-THF, which were acquired for the contrast conditions that make each of the polymer species "visible" during the measurement. The insert in Fig. 3 shows the same results in a Kratky plot. The results shown in Fig. 3 were measured at the BL-15 Taikan beamline at J-PARC. The results from individual polymer solutions in d-THF are shown by symbols in Fig. 3. Both the sPS and the PEGDME20K are in coil form at 110 °C.

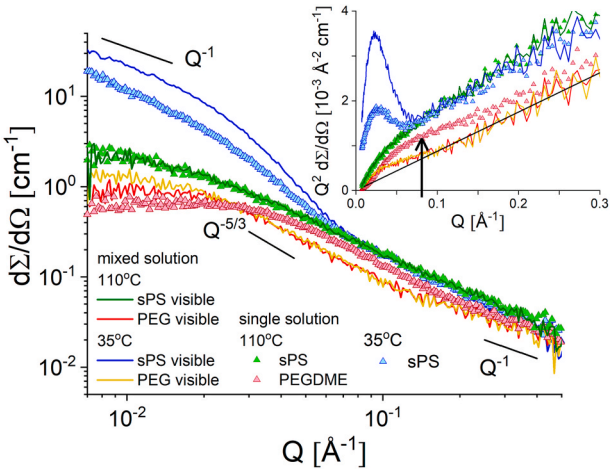

Fig. 3. Small angle scattering cross sections measured on sPS (φ_p = 5 %) and PEGDME20k (φ_p = 1 %) in common d-THF solution at decreasing temperature, from single coil conformation at 110 °C to gelation of sPS at 35 °C, in parallel with the results obtained on individual polymer solutions in d-THF. The sPS/PEGDME20K/d-THF ternary system was measured under different contrast conditions that make one of the two polymer components visible, as indicated in the legend. The solid black lines show the power law behavior of the scattering intensity in different Q-ranges. The inset shows the same results in a Kratky-plot, with the black line representing the signal from a rod-like morphology and the vertical arrow indicating the structure-factor effect for the PEGDME alone in solution.

The scattering characteristics typical of semiflexible coils are indicated by the power laws, similar to Fig. 2. The PEGDME20K result for φ_P = 1 % agrees very well with the result reported in Fig. 2, measured with the KWS-2 SANS diffractometer at 30 °C, and thus shows a structure factor effect superimposed on the polymer form factor signal. It can be assumed that the scattering pattern of the sPS is also influenced by correlation effects between the polymer coils, although no detailed experimental analysis was performed on sPS solutions with different φ_P. According to earlier SANS studies [23–25], sPS behaves like a worm-like chain in benzene, toluene, chloroform or naphthalene-based solvents at high temperatures.

At 35 °C, the sPS alone in solution provides a strong scattering signal at low Q that deviates significantly from single coil scattering. This indicates that some of the sPS chains have assembled into an elongated, possibly fibrillar morphology, as indicated by the Q^{-1} power law of intensity observed towards low Q, while most of the chains are still in the coil conformation, as no noticeable decrease in intensity is observed at high Q. The formation of the sPS-1D assemblies is driven by cooperative interactions between the sPS segments and the solvent molecules as the gelation temperature of the polymer is approached. The Q^{-1} power law behavior observed at low Q values indicates the formation of a fibrillar morphology as reported in Refs. [23,26], which may represent the junctions that promote the formation of the polymer gel.

The scattering of sPS from a joint solution with PEGDME20K in d-THF, measured at 110 °C under a contrast condition that renders the PEGDME20K "invisible", agrees with the scattering of sPS alone, indicating that the sPS is in single coil conformation at this temperature. The contrast condition that makes PEGDME20K "visible" and sPS "invisible" shows that the scattering pattern of PEGDME20K in single coil conformation is clearly different from that of PEGDME20K in simple THF solution for the same φ_P = 1 %: no structure factor effect is observed and the scattering properties are similar to those of very low φ_P in simple THF solution (Fig. 2). Thus, the correlation effects between PEGDME20K coils at φ_P = 1 % disappear in the presence of the "invisible" sPS in solution, and the scattering pattern only reveals the form factor of the PEGDME20K.

The Kratky plot of the results in the inset of Fig. 3 clearly shows that the PEGDME20K adopts a worm-like conformation in the joint THF solution with sPS at φ_P = 1 %: For the contrast condition visualizing the PEGDME20K, the same peculiarities are observed as for the single polymer solution at the much lower polymer concentration in THF, shown in Fig. 2b. The effect of the structure factor characteristic of the single polymer solutions at these high concentrations or affecting the sPS coils in the mixed solution, as evidenced by the experimental results measured under the sPS contrast, is indicated by the vertical arrow in the inset of Fig. 3. These effects clearly lead to deviations from the scattering pattern characteristic of a worm-like coil conformation.

A schematic representation of the conformation of the polymers in single and joint solution for different scattering contrast conditions is suggested in the sketch in Fig. 4.

The h-sPS/d-THF sample was additionally characterized on the KWS-2 diffractometer, complemented by in situ FTIR, simultaneously with SANS. The SANS patterns are consistent with those in Fig. 3. The conformational range of the FTIR spectra recorded simultaneously with SANS at two temperatures, 110 °C and 35 °C, is shown in Fig. 5. The spectra show the characteristic bands of sPS in amorphous coil form in solution at 110 °C (538 cm^{-1}) and in helical TTGG conformation of the junctions in gel form at 35 °C (549 cm^{-1} and 572 cm^{-1}). The configuration of the bands is similar to that reported in Ref. [22] in the study of sPS gelation in chloroform, benzene and toluene. The right inset in Fig. 5 shows the time evolution of the band at 572 cm^{-1} after reaching the temperature of 35 °C on the sample until its saturation, which shows that the gel is stabilized after about 15 min after reaching the set temperature, which is information used at the beginning of the acquisition and analysis of the SANS data. According to Ref. [44], gelation in SPS/o-dichlorobenzene and SPS/carbon tetrachloride systems is

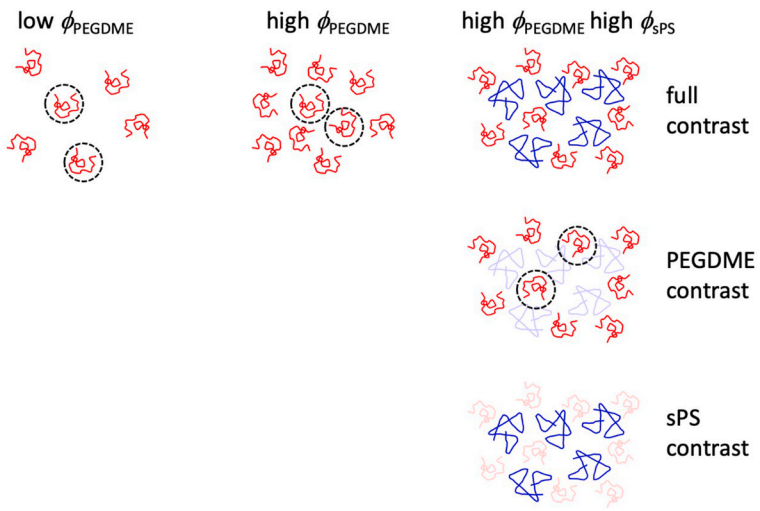

Fig. 4. Cartoon depicting the proposed single chain arrangement of PEGDME in THF in the low and high polymer concentration samples and the single chain arrangements of PEGDME and sPS as revealed by the SANS contrast matching experiments. The correlation effects between the PEGDME chains observed at high polymer concentration in THF alone were no longer observed when sPS was added, as shown in the right column.

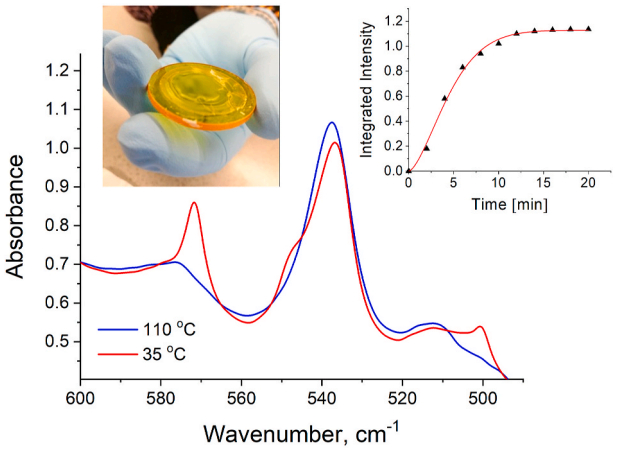

Fig. 5. IR spectra in the conformational band region of sPS in d-THF, measured at two temperatures, above and at the gelation point observed by DSC (Fig. 1). The FTIR measurements were performed in-situ, simultaneously with the SANS experiment. The left inset shows the aspect of the sample at the end of the experiment revealing the translucent polymer gel, while the right inset shows the temporal evolution of the integrated intensity of the band developing at 572 cm^{-1}.

completed within a few minutes at room temperature, whereas in SPS/chloroform it proceeds very slowly with a time scale of several tens of hours or longer.

With all this information about the gelation/melting temperatures and the onset of gelation associated with a conformational change of sPS between a single coil and a helix in individual or joint polymer solutions, a detailed simultaneous SANS and in situ FTIR characterization of sPS-PEGDME20K in a joint solution of d-THF was performed by lowering the temperature from 110 °C to 20 °C, using the contrast matching for SANS. Selected FTIR spectra at these two temperatures are shown in Fig. 6, corresponding to the different contrast conditions used in SANS. The region of the spectra corresponding to the conformational bands of sPS (580 cm^{-1} to 520 cm^{-1}) shows essentially the same patterns as those shown in Fig. 5 for the contrast conditions that visualize sPS in the SANS experiment (h-sPS). In the presence of PEGDME20K, the h-sPS bands corresponding to the helical conformation at 20 °C are more pronounced, which is in good agreement with the DSC observations showing that gelation occurs in the joint sPS and PEGDME20K solution in THF at higher temperature than in the case of only sPS in THF (Fig. 1).

The spectral region corresponding to the PEGDME conformational bands (1400 cm^{-1} to 1200 cm^{-1}), in which the characteristic bands of h-PEGDME should appear in amorphous (1352 cm^{-1}) and helical (1345 cm^{-1} and 1364 cm^{-1}) conformation [45], shows no qualitative change with decreasing temperature down to 20 °C, indicating that the PEGDME20K does not adopt a helical conformation below the gelation temperature of sPS. However, from the DSC observations, we can already infer that although the PEGDME20K molecules do not form a regular helical structure, segments of the long molecules can still adopt an elongated conformation and that they are entrapped by the fibrillar sPS aggregates after a co-assembly process with sPS driven by sPS gelation.

The SANS patterns shown in Fig. 7 were recorded simultaneously with the FTIR analysis under different contrast conditions that "visualize" either the sPS or the PEGDME20K. Both polymers are in a single coil conformation at 110 °C, as can be seen from the form factor scattering features. At 20 °C, the scattering features of polymer assemblies appear due to the gelation process driven by sPS. According to DSC and FTIR observations, these are structures formed jointly by sPS and PEGDME20K, with sPS adopting the crystalline helical conformation and PEGDME20K having an amorphous elongated conformation.

Two power laws can be recognized in the scattering patterns at medium and low Q ranges, especially under sPS contrast conditions: The Q^{-2} power law observed in the medium Q range turns into a Q^{-1} power law at low Q values, indicating the formation of elongated structures with a 1D overall aspect that exhibit a 2D aspect on a smaller length scale corresponding to the lateral size of the aggregates. Fibrillar or platelet-like morphologies result in such a scattering pattern. These polymer aggregates are mainly composed of helical sPS with elongated PEGDME20K segments sandwiched between sPS helices, which are the junctions of the polymer gel. Therefore, both sPS and PEGDME20K should have long segments that are still amorphous and extend away from the aggregating objects, resulting in the network-like character of the gel. At high Q, the power-law behavior of the scattering intensity for both contrast conditions suggests a single coil form factor, which could correspond to the larger coils still in solution and the smaller amorphous segments extending away from the polymer aggregates.

On the other hand, the fact that in the sPS contrast condition at low temperatures, the intensity at high Q decreases compared to the intensity at 110 °C suggests that a large number of sPS chains are already incorporated into the aggregates in helical conformation, reducing the volume fraction of the sample occupied by the polymer still in coil form. The observation that both patterns follow the same qualitative behavior

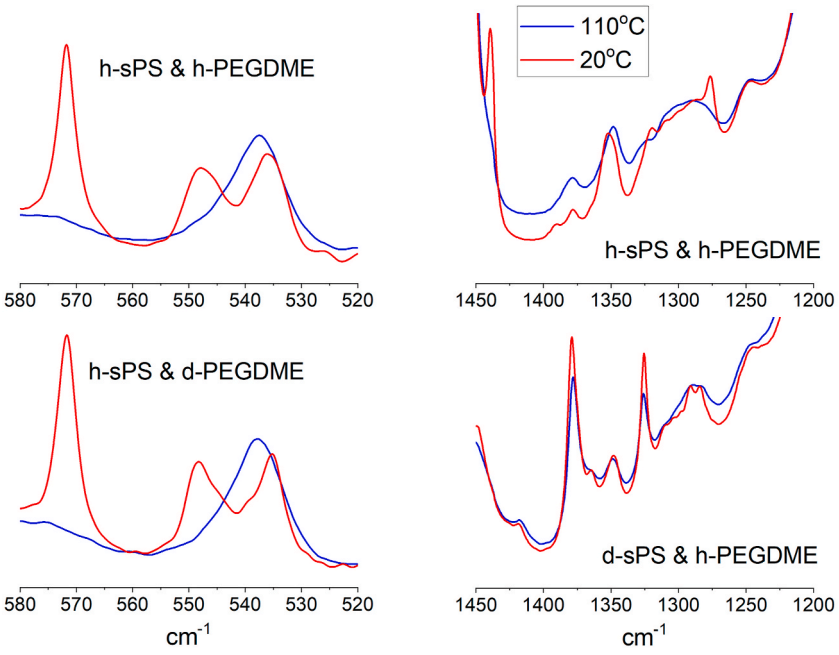

Fig. 6. Selected regions from the FTIR spectra measured at different temperatures simultaneously with SANS on a common sPS and PEGDME20K solution in d-THF, for different neutron contrast conditions, as indicated in the panels.

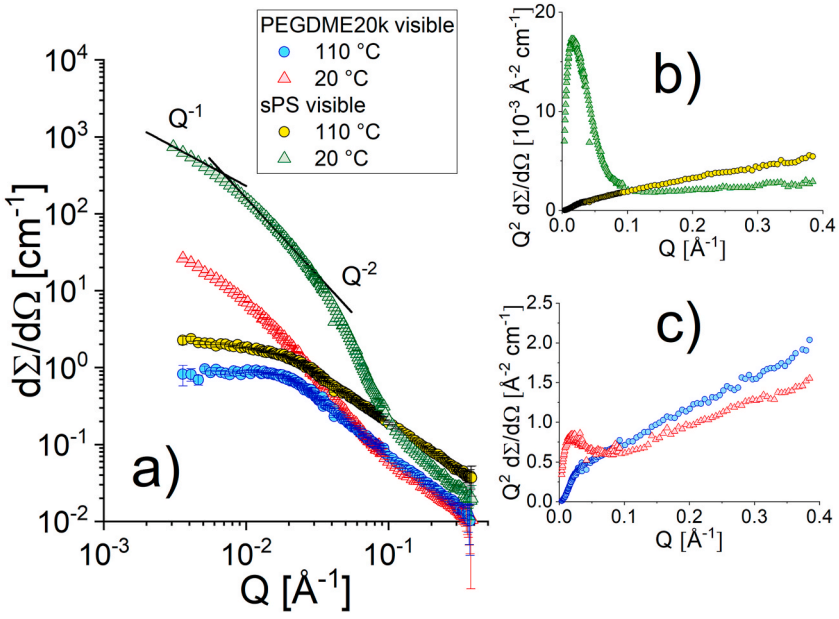

Fig. 7. Small angle scattering cross sections measured under different contrast conditions of sPS ($\varphi_p = 5$ %) and PEGDME20k ($\varphi_p = 1$ %) mixed in common d-THF solution at decreasing temperature from the single coil conformation regime at 110 °C to the gelation regime of sPS at 20 °C shown in log-log representation (a) and in as Kratky plots (b, c). The contrast conditions visualize always one of the two polymer components as indicated in the legend. The solid black lines show the power law behavior of the scattering intensity in different Q-ranges.

under sPS and PEGDME20K contrast conditions, differing only in intensity (which is much higher in the case of the "visible" sPS), suggests that sPS and PEGDME20K are uniformly distributed in the aggregates formed by association involving both polymer species. Since the contrast between the two polymer species in hydrogenated form and the deuterated THF is quite similar (Table 1), the difference in intensity can be attributed to the different volume fraction of the two polymer species within the aggregates. Assuming a homogeneous distribution of the two types of polymer molecules within the aggregates and also the compact aggregates, then

$$I(Q) \approx \varphi_{agg} \Delta\rho^2_{agg} = \Phi_{agg} \left(\varphi^{agg}_{sPS} \Delta\rho^{agg}_{sPS} + \varphi^{agg}_{PEGDME} \Delta\rho^{agg}_{PEGDME}\right)^2 \quad (6)$$

with φ_{agg} - the volume fraction of the sample occupied by the aggregates, $\Delta\rho_{agg}$ - the contrast between the aggregates and their surroundings, and the factors on the right-hand side of the equation within the paranthesis, which represent the volume fraction of an aggregate occupied by one of the two polymer species, multiplied by the corresponding contrast factor squared. Thus, for each contrast condition, one of the two terms on the right-hand side within the paranthesis disappears, so that the measured

intensity is proportional to the volume fraction of the "visible" polymer species within the aggregate. A rough estimate of the intensity at Q_{min} for each of the contrast conditions in Fig. 7 shows that the volume fraction of the aggregate occupied by sPS is about five times larger than that of PEGDME20K, which corresponds to the ratio between the two volume fractions of the polymers in the original joint solution. The co-assembly process thus leads to a homogeneous distribution of the two polymers within the aggregates.

The results of the SANS measurements performed on a joint sPS and PEGDME40K solution in THF at decreasing temperature between the single coil mode at 110 °C and the co-assembly regime at 10 °C are shown in Fig. 8. The Q range was extended to lower Q values compared to the previous SANS analyses. The same type of scattering features were observed as in the case of PEGDME20K. At very low Q values, a tendency towards an increase in intensity with respect to the Q^{-1} behavior can be assumed (vertical arrow mark), which could be related to the scattering from the large-scale network-like gel morphology.

In an early SANS study on physical gels formed by sPS in $CDCl_3$, the data were interpreted using a model combining mass and surface fractal features with the approach of Guinier and Kratky plots [46].

Motivated by the observation of the scattering features in the SANS patterns measured in the gel state, namely the observed Q^{-2} power law at medium Q, indicative of the 2D aspect of the aggregates at the lower size scale, and the Q^{-1} power law at low Q, characteristic of the overall 1D aspect of the aggregates at the larger length scale, for the simultaneous interpretation of the scattering data measured at 10 °C for the three contrast conditions (sPS visible, PEGDME40K visible and both polymers visible), a model combining the form factor of a long parallelepipedon [47] with the coil form factor at high Q values and a Q^{-3} power law in the very low Q range was used. The parallelepipedon form results in the Q^{-2} power law behavior of the scattering pattern at medium Q values, which changes to a Q^{-1} behavior towards lower Q values. The length of such one-dimensional aggregates in the overall aspect and the transition to the network generated by such cross-linking structures can be estimated from the Q value, where the increase in intensity occurs at very low Q and deviates from the Q^{-1} behavior. The coil form factor represents the scattering contribution at high Q, while the steeper power law at low Q comes from the contribution of gel morphology with larger length scale, most of which scatters outside the Q range covered in this experiment.

The parallelepipedon model that assumes a rectangular cross section and an elongated aspect was developed in Ref. [47]:

$$I(Q) = I_0 \frac{(l_a l_b l_c)^2}{4\pi} \int_0^{2\pi} \int_0^{\pi} \left[\frac{\sin(\pi Q l_a \sin\varphi \cos\psi)}{\pi Q l_a \sin\varphi \cos\psi}\right] \left[\frac{\sin(\pi Q l_b \sin\varphi \sin\psi)}{\pi Q l_b \sin\varphi \sin\psi}\right] \left[\frac{\sin(\pi Q l_c \cos\varphi)}{\pi Q l_c \cos\varphi}\right] \sin\varphi d\varphi \, d\psi \quad (7)$$

where I_0 is the forward scattering, which takes into account the contrast factor squared and the volume fraction of the scattering objects, l_a, l_b and l_c are the side lengths of the parallelepipedon, and φ and ψ are the polar and the azimuthal angles, respectively. Additional scattering contributions from the coils of the two polymers connecting the gel compounds or still in solution and the large-scale gel structure at high Q or low Q were added to Eq. (7). To simplify the model, the contribution from the coils was modelled using the unified equation (Eq. 2) for only one structural level with the exponent 5/3 and the main fitting parameters I_0coil and $R_g$coil, while the contribution from the gel at low Q was interpreted as P_3Q^{-3}, with the P_3 pre-factor as the fitting parameter.

The results of the fitting procedure applied to the data measured at 10 °C simultaneously for all contrast conditions are shown as lines in Fig. 9. The red lines indicate the global fitting results, while the blue and black solid lines represent the contribution of polymer aggregates for the visible PEGDME40K and sPS, respectively. The fitting procedure provided the three dimensions of the aggregates, l_a - the thickness, l_b - the

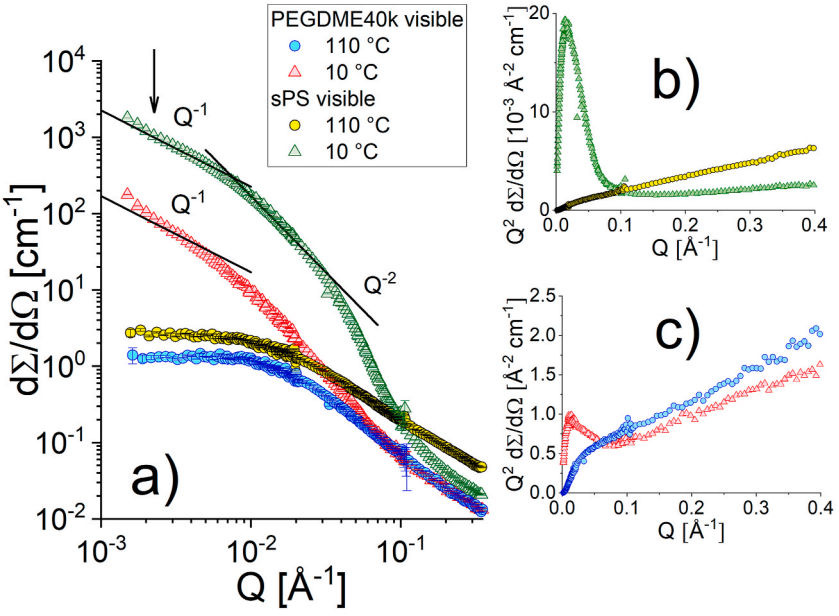

Fig. 8. Small angle scattering cross sections measured under different contrast conditions of sPS (φ_p = 5 %) and PEGDME40k (φ_p = 1 %) mixed in common d-THF solution at decreasing temperature from the single coil conformation at 110 °C to the gelation state of sPS at 10 °C; panels a, b, c and lines and symbols with the same meaning as in Fig. 7.

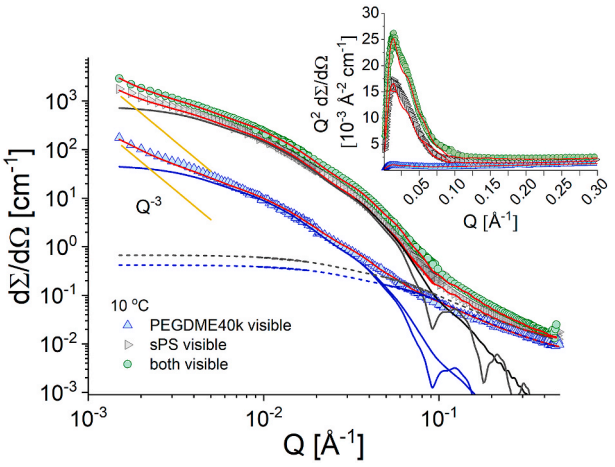

Fig. 9. Model interpretation of the SANS patterns of the aggregates formed by gelation of sPS and PEGDME40K in common solution in d-THF at 10 °C shown in log-log (main plot) and Kratky (inset plot) representations: the symbols are experimental data measured under different contrast conditions, as explained in the legend, while the red curves represent the results of simultaneous fitting of all three SANS patterns, as described in the text; the black and blue solid lines represent the scattering contribution of the aggregates (with and without 10% polydispersity in l_a size considered), while the dashed lines show the scattering contribution of the polymer coils; the additional contribution of the large-scale gel network is shown as a power law at low Q. (For interpretation of the references to colour in this figure legend, the reader is referred to the Web version of this article.)

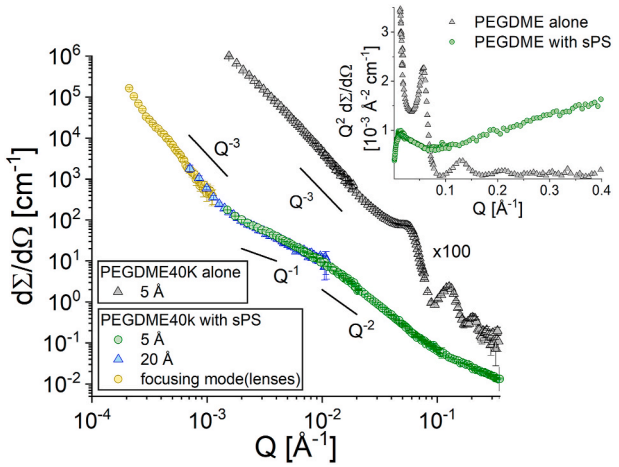

Fig. 10. SANS patterns of h-PEGDME40K morphology formed in d-THF (φ_{pol} = 3 %) collected at 10 °C (black symbols), in parallel with the scattering contribution of h-PEGDME40K (φ_{pol} = 1 %) (green/blue/yellow symbols), when co-assembled with d-sPS in common solution in d-THF (scattering from d-sPS was matched-out). The power law behavior of the scattering intensity in different Q-ranges is indicated as explained in the text. The inset shows the results measured over the conventional SANS-Q range in a Kratky plot. (For interpretation of the references to colour in this figure legend, the reader is referred to the Web version of this article.)

Table 2
Parameters delivered by the fitting procedure of the experimental data at 10 °C according to the model discussed in the text.

Parameter	contrastcondition	
	sPS visible	PEGDME40K visible
I_0 aggregates [cm^{-1}]	563.40 ± 22.35	28.59 ± 1.90
l_a, thickness [Å]	35.22 ± 0.99	35.22 ± 0.99
l_b, width [Å]	140.72 ± 3.55	140.72 ± 3.55
l_c, length [Å]	591.10 ± 22.34	591.10 ± 22.34
I_0coil [cm^{-1}]	0.34 ± 0.07	0.21 ± 0.04
$R_g$coil [Å]	62.60 ± 7.80	54.1 ± 6.90
P_3 [cm^{-1} Å^{-3}]	2.10E-6	2.5E-7

width and l_c - the length, and the forward scattering I_0, which depends on the SLD of the aggregates for the different contrast conditions considered, i.e. the volume fraction of the aggregate occupied by each polymer species. In addition, the R_g value of the polymer coils and their forward scattering were determined for each polymer species under the corresponding contrast conditions, as well as the pre-factor P_3 of the Q^{-3} power law at low Q value. Due to the good separation of the fitted morphologies on the length scale, the parameters determined by the model interpretation method are quite reliable. The structure and specific scattering parameters resulting from the fitting are listed in Table 2. The analysis of the "forward scattering" of the aggregates according to Eq. (2) shows that the fibrillar, board-like morphologies consist of approx. 83% sPS and 17% PEGDME40K, which roughly corresponds to the ratio of the concentrations of the two polymer species in the initial solution in THF. Thus, it can be assumed that segments of the PEGDME polymer are incorporated into the aggregated structure driven by the sPS gelation with the solvent molecules, and the fact that no PEGDME crystallization was observed suggests that the PEGDME segments are located between the sPS helices rather than forming well-defined domains within the aggregates.

The inset in Fig. 9 shows the experimental data and the overall results of the fit for all three contrast conditions considered in a Kratky plot. The model describes the scattering features shown in this plot quite well, although some discrepancies can be observed around Q = 0.03 Å^{-1}. However, considering that the model is a rough approximation of a real morphology that should be characterized by smearing factors of all side lengths specific to all contrast conditions, we can assume that the interpretation of the scattering data by the parallelepipedon model generally describes all observed features and the cooperative gelation of the two types of polymers quite well. The sPS effect on the behavior of PEGDME with high M_W is evident by comparing the scattering pattern of PEGDME40K (φ_{pol} = 1 %) co-assembled with sPS in common aggregates from THF solution with the scattering pattern of PEGDME40K alone (φ_{pol} = 3 %) in THF at 10 °C, as shown in Fig. 10. PEGDME alone forms a "house of cards" gel in THF, as indicated by the Q^{-3} power law behavior at medium Q, which consists of stacked lamellar structures at smaller length scale, as evidenced by the interlamellar correlation peak and higher order correlations at smaller length scale, as indicated by the scattering features observed at high Q. In the presence of sPS, smaller and softer structures appear, with the PEGDME molecules involved in the formation of fibrillar morphologies with a localized 2D aspect as a result of a cooperative gelation process controlled by sPS. These morphologies represent the junctions of a gel network that scatters at much lower Q values, as shown in Fig. 10. Using pinhole and focusing SANS data collected over a wide Q range, the contribution of PEGDME to scattering from the large-scale gel structure at very low Q values can be recognized.

4. Conclusions

Physical gelation of sPS in the presence of high M_W PEGDME from THF solution was studied by contrast variation SANS. Contrast matching was used to characterize the scattering contribution of each component in the ternary system and to follow the behavior of each polymer species during gelation process. The gelation and melting temperatures of mixed and individual polymer solutions in THF were determined by DSC. The formation and evolution of the structure and morphology at different gelation temperatures in transition from the single-coil conformation of the two polymer species at 110 °C to the ordered regular conformational of sPS in gel phase was additionally monitored in-situ by FTIR analysis of the samples simultaneously with SANS. A cooperative gelation process

of sPS and high M_W PEGDME was observed. sPS changes from the amorphous coil to the helical TTGG conformation when the gelation temperature is passed, forming fibrillar morphologies with a local 2D aspect, as revealed by the scattering data, due to cooperative interactions with the solvent molecules. These aggregates are the junction structures of the large-scale network morphology of the gel. The high molecular weight PEGDME transitions from the amorphous coil to an elongated amorphous conformation and incorporates into the fibrillar morphology together with the sPS during the gelation process. High M_W PEGDME alone in THF forms a "house of cards" gel consisting of stacked lamellar structures on a smaller length scale, as shown by the scattering data. Thus, in the presence of sPS, smaller and softer structures appear as a result of a cooperative gelation process controlled by sPS. According to other structural studies, the structure of sPS fibrils in gel form is identical to the structure of the co-crystalline phase of sPS δ (clathrates and intercalates). The incorporation of high M_W PEGDME into these aggregates thus leads to polymer nanocomposites that can render the sPS hydrophilic, a topic that should be the focus of future structural and morphological studies.

CRediT authorship contribution statement

Fumitoshi Kaneko: Supervision, Methodology, Investigation, Conceptualization. **Maria-Maddalena Schiavone:** Methodology, Investigation, Formal analysis, Data curation. **Hiroki Iwase:** Methodology, Investigation. **Shin-ichi Takata:** Methodology, Investigation. **Jürgen Allgaier:** Methodology, Investigation. **Aurel Radulescu:** Writing – original draft, Supervision, Methodology, Investigation, Formal analysis, Data curation, Conceptualization.

Declaration of competing interest

The authors declare the following financial interests/personal relationships which may be considered as potential competing interests: Aurel Radulescu reports administrative support, equipment, drugs, or supplies, and travel were provided by Forschungszentrum Jülich GmbH. If there are other authors, they declare that they have no known competing financial interests or personal relationships that could have appeared to influence the work reported in this paper.

Data availability

Data will be made available on request.

Acknowledgement

The authors thank Toshiaki Morikawa (CROSS) for providing technical support in the SANS experiment at J-PARC MLF. The SANS experiment at the Materials and Life Science Experimental Facility of the J-PARC was performed under a user program (Proposal No. 2016A0198). The help from Tobias Schrader (Forschungszentrum Jülich GmbH) for preparing the FTIR measurements is kindly acknowledged.

References

[1] N. Ishihara, T. Seimiya, M. Kuramoto, M. Uoi, Macromolecules 19 (1986) 2464–2465.
[2] G. Guerra, V.M. Vitagliano, C. DeRosa, V. Petraccone, P. Corradini, Macromolecules 23 (1990) 1539–1544.
[3] Y. Chatani, Y. Shimane, Y. Inoue, T. Inagaki, T. Ishioka, T. Ijitsu, T. Yukinari, Polymer 33 (1992) 488–492.
[4] E. Bhoje Gowd, K. Tashiro, C. Ramesh, Prog. Polym. Sci. 34 (2009) 280–315.
[5] O. Tarallo, M.M. Schiavone, V. Petraccone, C. Daniel, P. Rizzo, G. Guerra, Macromolecules 43 (2010) 1455–1466.
[6] O. Tarallo, M.M. Schiavone, V. Petraccone, Eur. Polym. J. 46 (2010) 456–464.
[7] O. Tarallo, M.M. Schiavone, V. Petraccone, Polymer 52 (2011) 1426–1435.
[8] Y. Uda, F. Kaneko, T. Kawaguchi, Polymer 45 (2004) 2221–2229.
[9] Y. Uda, F. Kaneko, T. Kawaguchi, Macromolecules 38 (2005) 3380–3385.
[10] P. Rizzo, S. Della Guardia, G. Guerra, Macromolecules 37 (2004) 8043–8049.
[11] C. Daniel, A.R. Albunia, C. D'Aniello, P. Rizzo, V. Venditto, G. Guerra, Journal of the European Optical Society - Rapid Publications 4 (2009) 09037.
[12] P. Stegmaier, A. De Girolamo Del Mauro, V. Venditto, G. Guerra, Adv. Mater. 17 (2005) 1166–1168.
[13] M. Giordano, M. Russo, A. Cusano, G. Mensitieri, G. Guerra, Sensor. Actuator. B 109 (2005) 177–184.
[14] P. Rizzo, C. Daniel, G. Guerra, Macromolecules 43 (2010) 1882–1887.
[15] G. Milano, G. Guerra, Prog. Mater. Sci. 54 (2009) 68–88.
[16] F. Kaneko, K. Sasaki, Macromol. Rapid Commun. 32 (2011) 988–993.
[17] F. Kaneko, N. Seto, S. Sato, A. Radulescu, M.M. Schiavone, J. Allgaier, K. Ute, Chem. Lett. 44 (2015) 497–499.
[18] S. Sato, T. Kawaguchi, F. Kaneko, Macromol. Symp. 369 (2016) 114–118.
[19] S. Sato, Y. Yamamoto, F. Kaneko, Chem. Lett. 48 (2019) 177–180.
[20] F. Kaneko, N. Seto, S. Sato, A. Radulescu, M.M. Schiavone, J. Allgaier, K. Ute, J. Appl. Crystallogr. 49 (2016) 1420–1427.
[21] H. Shimizu, T. Wakayame, R. Wada, M. Okabe, F. Tanaka, Polym. J. 37 (2005) 294–298.
[22] M. Kobayashi, T. Yoshioka, M. Imai, Y. Itoh, Macromolecules 28 (1995) 7376–7385.
[23] C. Daniel, M.D. Deluca, J.-M. Guenet, A. Brulet, A. Menelle, Polymer 37 (1996) 1273–1280.
[24] C. Daniel, A. Menelle, A. Brullet, J.-M. Guenet, Polymer 38 (1997) 4193–4199.
[25] S. Malik, C. Rochas, M. Schmutz, J.-M. Guenet, Macromolecules 38 (2005) 6024–6030.
[26] C. Daniel, S. Giudice, G. Guerra, Chem. Mater. 21 (2009) 1028–1034.
[27] C. Daniel, G. Guerra, P. Musto, Macromolecules 35 (2002) 2243–2251.
[28] J. Mochizuki, T. Sano, T. Tokami, H. Itagaki, Polymer 67 (2015) 118–127.
[29] K. Senoo, S. Matsuda, S. Kohjiya, e-Journal of Soft Materials 2 (2006) 31–36.
[30] X. Wang, S.C. Jana, Langmuir 29 (2013) 5589–5598.
[31] B. Hammouda, D.L. Ho, S. Kline, Macromolecules 37 (2004) 6932–6937.
[32] C.H. Hövelmann, S. Gooßen, J. Allgaier. Macromolecules 50 (2017) 4169–4179.
[33] S. Takata, J. Suzuki, T. Shinohara, T. Oku, T. Tominaga, K. Ohishi, H. Iwase, T. Nakatani, Y. Inamura, T. Ito, JPS Conf. Proc. 8 (2015) 036020.
[34] A. Radulescu, V. Pipich, H. Frielinghaus, M.S. Appavou, J. Phys. Conf. 351 (2012) 012026.
[35] A. Radulescu, N.K. Szekely, M.S. Appavou, V. Pipich, T. Kohnke, V. Ossovyi, S. Staringer, G.J. Schneider, M. Amann, B. Zhank-Haagen, G. Brandl, M. Drochner, R. Engels, R. Hanslik, G. Kemmerling, J. Vis. Exp. 118 (2016) e54639.
[36] Y. Qu, L. Li, G. Lu, X. Zhou, Q. Su, W. Xu, S. Li, J. Zhang, X. Yang, Polym. Chem. 3 (2012) 3301–3307.
[37] P. Shaiju, N. Sanjeeva Murthy, E. Bhoje Gowd, Macromolecules 49 (2016) 224–233.
[38] S.H. Nguyen, D. Berek, I. Capek, O. Chiantore, J. Polym. Sci. Polym. Chem. 38 (2000) 2284–2291.
[39] O. Kratky, G. Porod, Rec. Trav. Chim. Pays-Bas 68 (1949) 1106–1122.
[40] G. Beuacage, S. Rane, S. Sukumaran, M.M. Satkowski, L.A. Schechtman, Macromolecules 30 (1997) 4158–4162.
[41] G. Beaucage, J. Appl. Crystallogr. 28 (1995) 717–728.
[42] B. Hammouda, J. Appl. Crystallogr. 43 (2010) 1474–1478.
[43] R. Ramachandran, G. Beaucage, A.S. Kulkarni, D. McFaddin, J. Merrick-Mack, V. Galiatsos, Macromolecules 41 (2008) 9802–9806.
[44] M. Kobayashi, T. Yoshioka, M. Imai, Y. Itoh, Physica B 213&214 (1995) 734–736.
[45] M. Kobayashi, K. Kitagawa, Macromol. Symp. 114 (1997) 291–296.
[46] M. Kobayashi, T. Yoshioka, T. Kozasa, K. Tashiro, J. Suzuki, S. Funahashi, Y. Izumi, Macromolecules 27 (1994) 1349–1354.
[47] J.S. Pedersen, Adv. Colloid Interface Sci. 70 (1970) 171–210.